

Time-Dependent Impact of Irreversible Electroporation on Pathology and Ablation Size in the Porcine Liver: A 24-Hour Experimental Study

Technology in Cancer Research & Treatment
Volume 18: 1-9
© The Author(s) 2019
Article reuse guidelines:
sagepub.com/journals-permissions
DOI: 10.1177/1533033819876899
journals.sagepub.com/home/tct


Jantien A. Vogel, MD, MSc¹, Eran van Veldhuisen, BSc¹ ,
Lindy K. Alles, BSc², Olivier R. Busch, MD, PhD¹,
Frederike Dijk, MSc, PhD³, Thomas M. van Gulik, MD, PhD^{1,2},
Goos M. Huijzer², Marc G. Besselink, MD, MSc, PhD¹,
Krijn P. van Lienden, MD, PhD⁴, and Joanne Verheij, MD, PhD³

Abstract

Irreversible electroporation causes cell death through low frequency, high voltage electrical pulses and is increasingly used to treat non-resectable cancers. A recent systematic review revealed that tissue damage through irreversible electroporation is time-dependent, but the impact of time on the ablation zone size remains unknown. Irreversible electroporation ablations were performed hourly during 24 consecutive hours in the peripheral liver of 2 anaesthetized domestic pigs using clinical treatment settings. Immediately after the 24th ablation, the livers were harvested and examined for tissue response in time based on macroscopic and microscopic pathology. The impact of time on these outcomes was assessed with Spearman rank correlation test. Ablation zones were sharply demarcated as early as 1 hour after treatment. During 24 hours, the ablation zones showed a significant increase in diameter ($r_s = 0.493$, $P = .014$) and total surface ($r_s = 0.499$, $P = .013$), whereas the impact of time on the homogeneous ablated area was not significant ($r_s = 0.172$, $P = .421$). Therefore, the increase in size could mainly be attributed to an increase in the transition zone. Microscopically, the ablation zones showed progression in cell death and inflammation. This study assessed the dynamics of irreversible electroporation on the porcine liver during 24 consecutive hours and found that the pathological response (ie, cell death/inflammation), and ablation size continue to develop for at least 24 hours. Consequently, future studies on irreversible electroporation should prolong their observation period.

Keywords

electroporation, liver, cell death, pilot study, pathology

Abbreviations

H&E, hematoxylin and eosin; IRE, irreversible electroporation; IQR, interquartile range

Received: October 29, 2018; Revised: April 30, 2019; Accepted: June 14, 2019.

¹ Department of Surgery, Cancer Center Amsterdam, Amsterdam UMC, University of Amsterdam, Amsterdam, the Netherlands

² Department of Experimental Surgery, Cancer Center Amsterdam, Amsterdam UMC, University of Amsterdam, Amsterdam, the Netherlands

³ Department of Pathology, Cancer Center Amsterdam, Amsterdam UMC, University of Amsterdam, Amsterdam, the Netherlands

⁴ Department of Interventional Radiology, Cancer Center Amsterdam, Amsterdam UMC, University of Amsterdam, Amsterdam, the Netherlands

Corresponding Authors:

Joanne Verheij, Department of Pathology, Cancer Center Amsterdam, Amsterdam UMC, University of Amsterdam, room M2-133, Amsterdam, the Netherlands.
Email: j.verheij@amc.nl

Eran van Veldhuisen, Department of Experimental Surgery, Cancer Center Amsterdam, Amsterdam UMC, University of Amsterdam, Meibergdreef 9, Amsterdam, Noord-Holland, 1105 AZ, the Netherlands.
Email: e.vanveldhuisen@amc.nl



Introduction

New treatment options such as irreversible electroporation (IRE) are emerging for the treatment of locally unresectable tumors. Irreversible electroporation achieves tumor cell death through the appliance of low frequency, high voltage electrical pulses.¹ Clinically, the use of IRE is being investigated in pancreatic cancer,²⁻⁵ liver cancer,^{6,7} perihilar cholangiocarcinoma,⁸ renal tumors,⁹ and prostate cancer.^{10,11} It is believed that IRE induces apoptosis through permeabilization of cell membranes, caused by a disturbance of the membrane potential, which results in free diffusion of cell contents rather than causing thermal damage.¹ However, both thermal and nonthermal effects are seen upon histological examination of IRE-treated tissue; therefore, the mechanism of work of IRE is thought to be based on a combination of these effects.¹²

Preclinical research has aimed to clarify the mechanism of IRE and thereby to optimize treatment parameters, but consensus is lacking. Nevertheless, IRE shows promising results in the treatment of malignancies, when patients are not eligible for resection due to local invasive growth of the tumor into vital structures such as blood vessels and bile ducts.¹³ These structures have shown to be vulnerable to thermal damage, whereas no significant damage is reported when performing IRE with these structures traversing the ablation zones.¹³

Previous experimental studies report on a dynamic tissue response after IRE. Upon histological examination, only non-specific signs of cell death are observed directly after treatment (ie, congestion, hemorrhagic infiltration). Several hours later, this is followed by an inflammatory response (ie, infiltration of neutrophils) and complete cell death.¹⁴ Despite this extensive pathological response,¹⁴ signs of clinical discomfort or impairment of organ function are reported as transient and relatively mild following ablation with IRE.¹⁵⁻¹⁷ However, complete cell death is hard to determine, and predictability of the distribution and development of the ablation zone remains challenging. Previously published preclinical studies often report histological evaluation at a fixed interval, often 4 to 6 hours after IRE. However, a recent systematic review suggested that the impact of IRE continues beyond this time interval.¹⁴ As a result, it is not known whether the ablation zone size remains stable or progresses in time. Tumor recurrences are still often reported,¹⁸ therefore, more insight in the mechanism of work of IRE is needed in order to allow for accurate predictability of the extent and distribution of the ablation zones.¹⁹

We aimed to investigate the dynamics of the pathological response of IRE in the porcine liver during 24 hours with the goal to obtain better insight in the time-dependent mechanism of action of IRE and to support the design of future experimental studies with IRE.

Methods

This experiment was performed in porcine livers, due to the close relation of size and tissue properties between porcine and human liver.

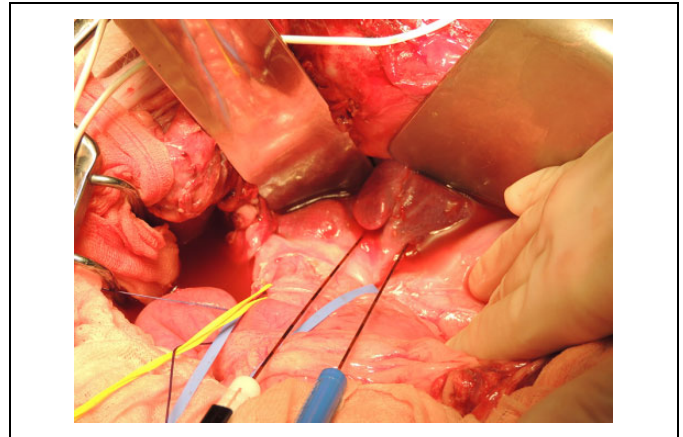


Figure 1. Open IRE procedure of porcine liver following midline laparotomy. IRE indicates irreversible electroporation.

Animal Model

Following a protocol approved by the institution's Animal Ethics Committee, IRE ablations were performed in the liver periphery of 2 domestic Yorkshire landpigs weighing approximately 50 kg (van Beek SPF Varkens B.V., Putten, the Netherlands). The animals were sedated with intramuscular ketamine (10-15 mg/kg), midazolam (1-1.5 mg/kg), and atropine (1.5 mL/50 kg). After intubation, anesthesia was maintained through inhaled isoflurane (2%-4%) and intravenous ketamine (2 mg/kg/h), sufentanil (5-10 mg/kg/h), midazolam (1-2 mg/kg/h), and rocuronium (2-2.5 mg/kg/h). Before IRE, intravenous bolus injections of rocuronium (1-1.5 mg/kg) were administered for complete muscle relaxation. The animal was placed in the supine position and the liver was exposed through a midline laparotomy (Figure 1).

Irreversible Electroporation Procedure

Twenty-four ablations were performed with 1-hour interval (12 ablations per liver, with intervals of 1 hour per ablation, as shown in Figure 2).

Typically, two 19-gauge Nanoknife electrodes (Angiodynamics, Latham, New York) were randomly positioned in the liver, perpendicular to the liver surface under ultrasound guidance, with a fixed interelectrode distance of 1.5 cm (using spacers) and an exposed tip of 1.5 cm, thus, ranging from 1 to 2.5 cm from the liver surface. Ablations were performed using electrocardiogram synchronization and clinical treatment settings, that is, 90 pulses were delivered per ablation with a pulse length of 90 μ s and a frequency of approximately 90 pulses/min, with an electric field strength of 1500 V/cm as previously described by Martin *et al.*²⁰ Ablations were performed in a way that overlap of the ablation zones was prohibited. A summary of the IRE parameters is shown in Supplementary File 1.

After each ablation, the electrodes were removed and repositioned, while the location of the electrodes was visualized with plastic catheters and the time of the ablation was marked

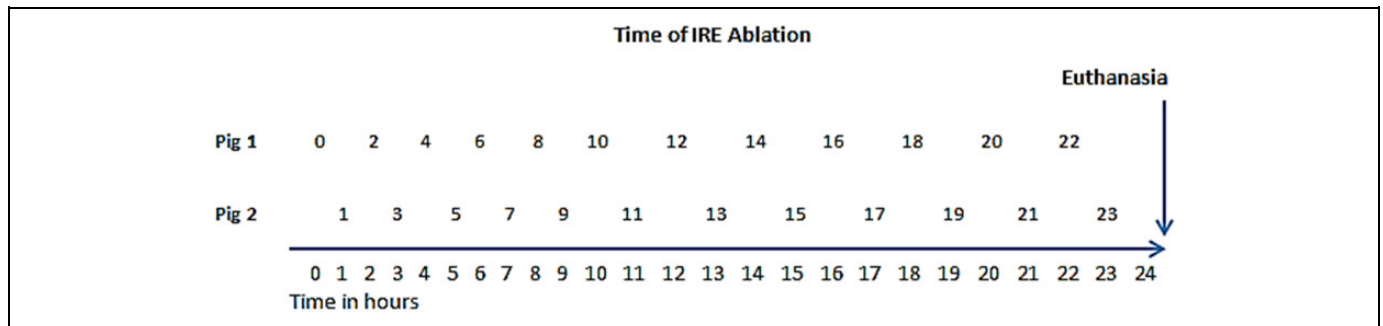


Figure 2. Time diagram of IRE ablations and euthanasia of treated pigs. IRE indicates irreversible electroporation.

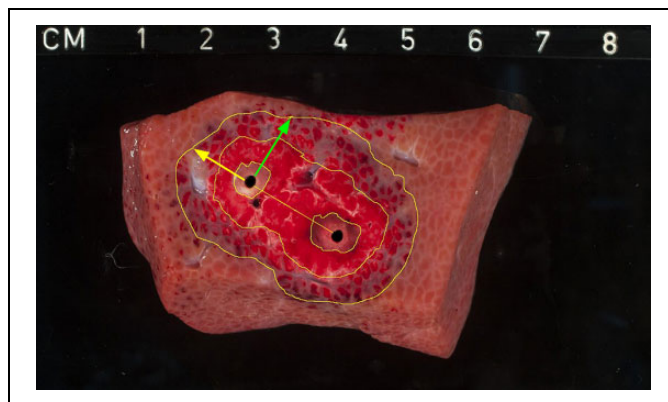


Figure 3. Gross pathology of ablation zone 21 hours after treatment. The ablation zone shows marked discoloration, with hemorrhagic infiltration and central zones of white coagulation. The periphery of the lesion shows a transition zone of vital tissue admixed with nonvital tissue. Green arrows indicating perpendicular distance from electrode to the edge of the ablation zone. Yellow arrows indicating parallel distance from electrode to the edge of the ablation zone. Numbers indicating various dimensions of the ablation zone, 1: zone of thermal damage; 2: homogeneous zone; 3: transition zone.

on the liver surface. Between ablations, the core temperature of the animals was stabilized by closing of the abdomen, blanket covering, and bair huggers when necessary. Vital parameters (ie, heart rate, blood pressure) were monitored throughout the experiment by senior technicians. Immediately after the last ablation, the animals were killed by exsanguination during full anesthesia and the livers were harvested. Fresh specimens were sliced perpendicular to electrode placement, exactly in the middle of the active tip area, at 1 cm distance from the liver capsule and after gross examination fixated in formalin, embedded in paraffin and hematoxylin and eosin (H&E) stained. The measurements of each ablation zone were determined in all specimens. Images of gross pathology were digitally analyzed (ImageJ, 1.48v, National Institutes of Health, Bethesda, MD, USA) and were divided into zones based on macroscopy. In addition, the distance between the electrodes and the edge of the ablated area were determined in 2 directions (parallel and perpendicular to the electrodes; Figure 3).

Specimens were microscopically evaluated by an experienced liver pathologist for histological response following IRE.

Statistical Analysis

Continuous data are presented as mean and standard deviation in case of a normal distribution or as median and interquartile range (IQR) in case of a non-normal distribution, while dichotomous data are presented as proportions. Normality of data was tested using the Shapiro-Wilk test. Spearman rank correlation test was used to determine the impact of time on the gross pathological outcomes. These results are displayed as correlation coefficients (r_s) with corresponding P values. A 2-tailed P value $<.05$ was considered statistically significant. Microscopic development was not statistically analyzed but solely described. Statistical analyses were performed using IBM SPSS statistics version 24.0 (IBM, Armonk, NY, USA).

Results

Experiment

Twenty-four ablations were performed in 2 *in vivo* pig livers with 1-hour interval. Twelve ablations were performed per liver. Both animals survived the procedure until the time of euthanasia and complete ablations were delivered in all cases. No adverse events during treatment were observed and the vital parameters of the animals remained stable throughout the 24-hour period.

Gross Pathology

Gross pathologic evaluation of the ablation zones showed well-demarcated lesions as early as 1 hour after treatment. The created lesions were characterized by red discoloration, with zones of white coagulation surrounding the electrodes. Traversing blood vessels and bile ducts remained structurally intact. On gross pathologic evaluation, multiple zones could be identified within the IRE lesions (Figure 3) and are as follows:

1. Zone directly surrounding the electrodes. White zone of coagulative necrosis which could presumably be attributed to direct thermal injury.
2. Homogeneous zone. Zone of extensive red discoloration and hemorrhagic infiltration, with loss of hepatic architecture. Complete cell death is seen within this region.

Table 1. Progression of Ablation Zone Sizes Over 24 Hours.^a

Time	Z1	Z2	HZ	TZ	TS	AAT	ø
24	28.3	28.6	342.6	424.0	766.6		40.0
23	14.2	14.8	306.9	179.0	485.9	745.2	30.0
22	21.1	32.5	336.8	406.5	743.3		36.2
21	14.4	29.9	116.9	297.5	414.4		31.7
20	27.6	15.2	187.1	132.4	319.5	484.2	29.0
19	27.0	15.4	160.6	138.5	299.1		26.1
18	77.1	15.1	285.9	277.9	563.8		32.2
17	6.4	20.6	104.9	191.8	296.7		23.9
16	34.9	18.8	167.1	147.2	314.3		23.9
15	23.1	9.0	222.7	95.8	318.5		25.1
14	8.5	25.2	144.0	239.3	383.3		25.9
13	10.1	11.9	207.2	256.9	464.1		30.8
12	11.9	6.0	160.9	206.0	366.9		26.3
11	9.7	5.6	223.9	154.6	378.5		31.4
10	8.0	6.0	205.5	153.3	358.8		26.8
9	7.9	10.8	293.4	168.6	462.0		30.8
8	12.2	6.9	200.1	187.0	387.1		26.1
7	4.6	11.0	264.1	71.6	335.7		28.2
6	6.1	15.6	163.1	183.7	346.8		23.9
5	11.0	0.0	175.7	138.6	314.3		25.4
4	1.7	8.1	351.0	37.2	388.2		25.9
3	8.3	10.1	108.9	250.4	359.3		27.3
2	6.6	6.3	218.2	88.1	306.3		24.2
1	5.8	12.8	134.5	179.4	313.9		25.2

Abbreviations: AAT, additional ablated tissue exceeding the planned ablation zone in mm²; HZ, homogeneous ablation zone in mm²; TS, total ablation zone surface in mm²; TZ, transition zone; Z1, zone around electrode 1 in mm²; Z2, zone around electrode 2 in mm²; ø, total ablation zone diameter in millimeters (HZ + TZ).

^aTime in hours.

- Transition zone between treated and nontreated tissue, which consists of vital tissue admixed with cell death. Macroscopically, these zones are characterized by mixed pale and red discoloration but with normal hepatic architecture. In some tissue samples, the transition zone exceeded the planned ablation zone volume, presumably caused by redistribution of the electric field. This was defined as “additional ablated tissue.”

Ablation Zone Measurements

The median diameter of the total ablation zones (homogenous zone + transition zone + area of thermal damage) was 26.6 mm (IQR 25.3-30.8), which showed a significant increase in time over 24 hours ($r_s = 0.493$, $P = .014$). Ablation zone diameters are shown in Table 1. Figure 4 gives a graphical overview of the progression of the ablation zone diameters measured over 24 hours.

For other parameters such as the distance of the electrode tips to the edge of the ablated area, the influence of time on these outcomes was significant. Transversally to the electrode placement, the median distance of the electrodes to the edge of the ablated area was 5.6 mm (IQR 5.20-6.70). This distance increased significantly over 24 hours ($r_s = 0.441$, $P = .031$).

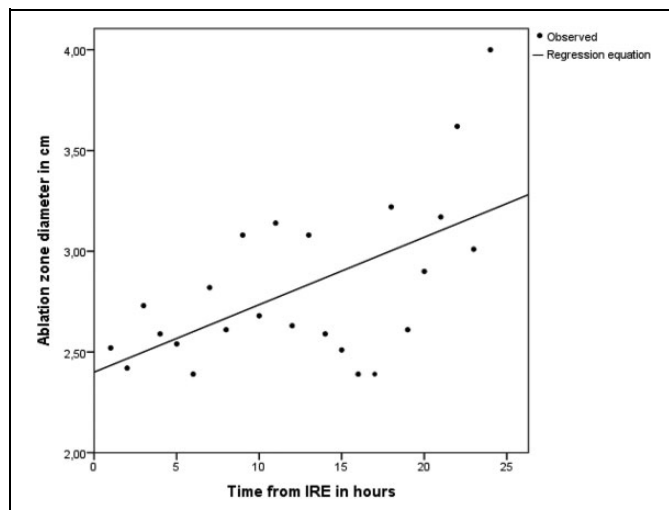


Figure 4. Diagram showing progression of the ablation zone diameter in time.

Perpendicular to the electrode placement, the median distance from the electrode to the edge of the ablated area was 0.76 cm (IQR 0.68-0.88). Also this distance increased significantly ($r_s = 0.417$, $P = .043$). Likewise, for the total surface of the ablation zone (macroscopic homogeneous plus transition zone plus additional ablated area), the influence of time showed a time-dependent impact ($r_s = 0.499$, $P = .013$). However, the progression in time of the homogeneous surface of the ablation zone was not significant ($r_s = 0.172$, $P = .421$).

The data on the measurements of the multiple divisions of the ablation zone over 24 hours are summarized in Tables 1 and 2.

Multiple lesions showed involvement of vascular structures upon histological examination, without a direct effect on the ablation zone. However, in 2 of the 24 lesions, an aberrant ablation zone was seen as shown in Figures 5 and 6. These zones showed a comparable gross pathological response with the gross proportion of the other lesions, however, the distribution of these ablation zones was aberrant. The lesion as shown in Figure 5 is enclosed by 2 large vascular structures and shows a heterogeneous distribution of the ablation zone with an additional ablated area.

Another aberrant lesion showed an incomplete ablation, as a rim of vital tissue was observed between the electrodes (Figure 6).

Given the fact that a plateau phase was not observed after 24 hours (ie, the ablation zone still demonstrated an increase in size), it is likely that the progression of the ablation zones proceeds beyond 24 hours.

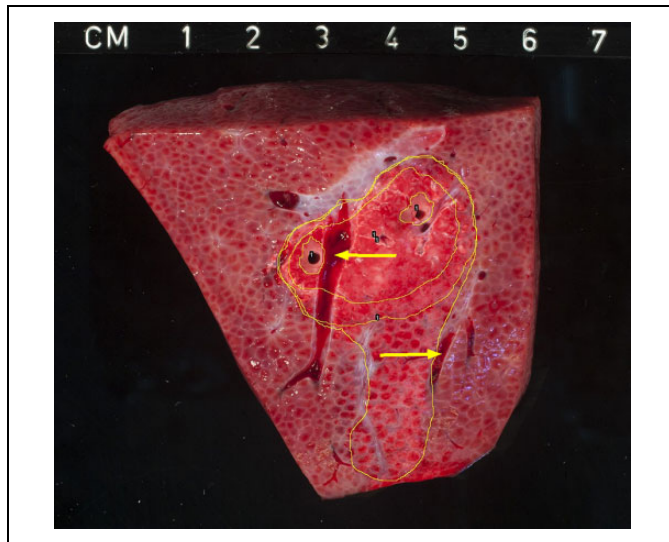
Microscopic Evaluation

Microscopic evaluation with H&E staining showed a clear-demarcated ablation zone with extensive hemorrhage as early as 1 hour after ablation (ie, the first evaluation). Cell death was

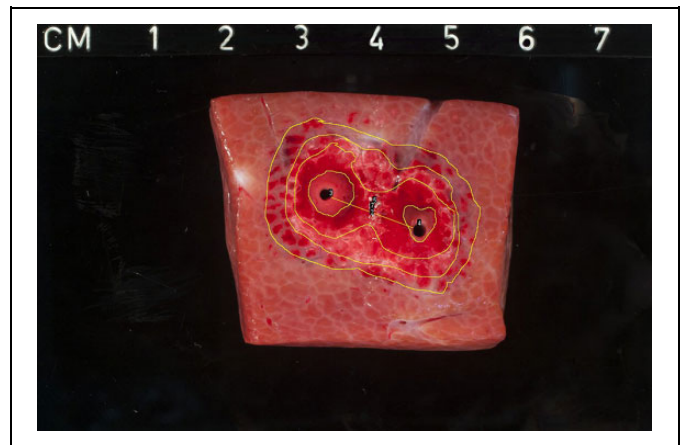
Table 2. Distance From the Electrodes to the Edge of the Ablated Area.

<i>t</i>	mPA	mPE
24	9.1	10.3
23	6.0	9.1
22	9.7	11.8
21	6.1	7.5
20	7.0	9.0
19	5.5	6.3
18	7.2	9.6
17	4.9	6.6
16	4.7	6.8
15	4.9	6.9
14	5.2	7.9
13	6.4	8.8
12	5.3	7.8
11	6.8	6.7
10	5.6	7.5
9	6.9	8.5
8	5.7	8.2
7	6.2	6.8
6	4.8	7.8
5	5.3	7.0
4	5.5	8.6
3	5.5	7.2
2	4.6	7.2
1	5.3	6.8

Abbreviations: mPA, mean distance from the electrodes to the edge of the ablated area parallel to the electrode placement in millimeters; mPE, mean distance from the electrodes to the edge of the ablated area perpendicular to the electrode placement in millimeters; *t*, time in hours.

**Figure 5.** Gross-pathologic evaluation 23 hours after ablation. The ablated tissue shows a well-demarcated ablation zone, with a heterogeneous distribution as compared to the other tissue samples. Yellow arrows indicating vascular structures.

difficult to objectify at this moment of evaluation, yet cells showed premature signs of apoptosis/necrosis (ie, congestion of sinusoidal spaces), see Figure 7A.

**Figure 6.** Gross-pathologic image of porcine liver tissue 19 hours after IRE. The ablation zone shows 2 macroscopically different transition zones of vital tissue admixed with non-vital tissue. IRE indicates irreversible electroporation.

After 4 hours, cell death was more pronounced and demonstrable. Irregular necrosis was seen at distance from the electrodes, while complete (confluent) necrosis in the proximity of the electrodes was observed. Moreover, the inflammatory response was initiated at this time of evaluation, which was characterized by the infiltration of neutrophils (Figure 7B).

Yet after 8 hours, although blood vessels and bile ducts remained structurally intact, thrombosis of microvasculature was seen. Satellite necrotic lesions were also seen, with influx of neutrophils (Figure 7C). Ten hours after ablation, the ablation zone showed an inhomogeneous aspect, with irregular distribution of necrosis admixed with vital hepatic tissue and peribiliary inflammation.

Thirteen hours after ablation, the ablated tissue showed limited vitality centrally within the ablation zone. Extensive tissue damage was present which was characterized by confluent necrosis of hepatocytes, with deeply eosinophilic cytoplasm and pyknotic nuclei.

After 18 hours, an occluding thrombus was seen in one of the vessels traversing the ablation zone. The vessel walls in the treated region showed signs of vasculitis, and likewise the traversing bile ducts showed signs of cholangitis. Traversing blood vessels did not show any response prior to this time of evaluation, demonstrating a later onset of tissue response in these structures compared to liver tissue (ie, hepatocytes). An extensive inflammatory response was seen in the entire ablation zone, with massive infiltration of neutrophils. The zones directly encasing the electrodes showed complete coagulative necrosis (Figure 7D).

Discussion

This is the first experimental study to systematically assess the correlation between time and histological outcomes following IRE in an *in vivo* porcine liver experiment over 24 hours with hourly assessment. Tissue damage through IRE was found to be

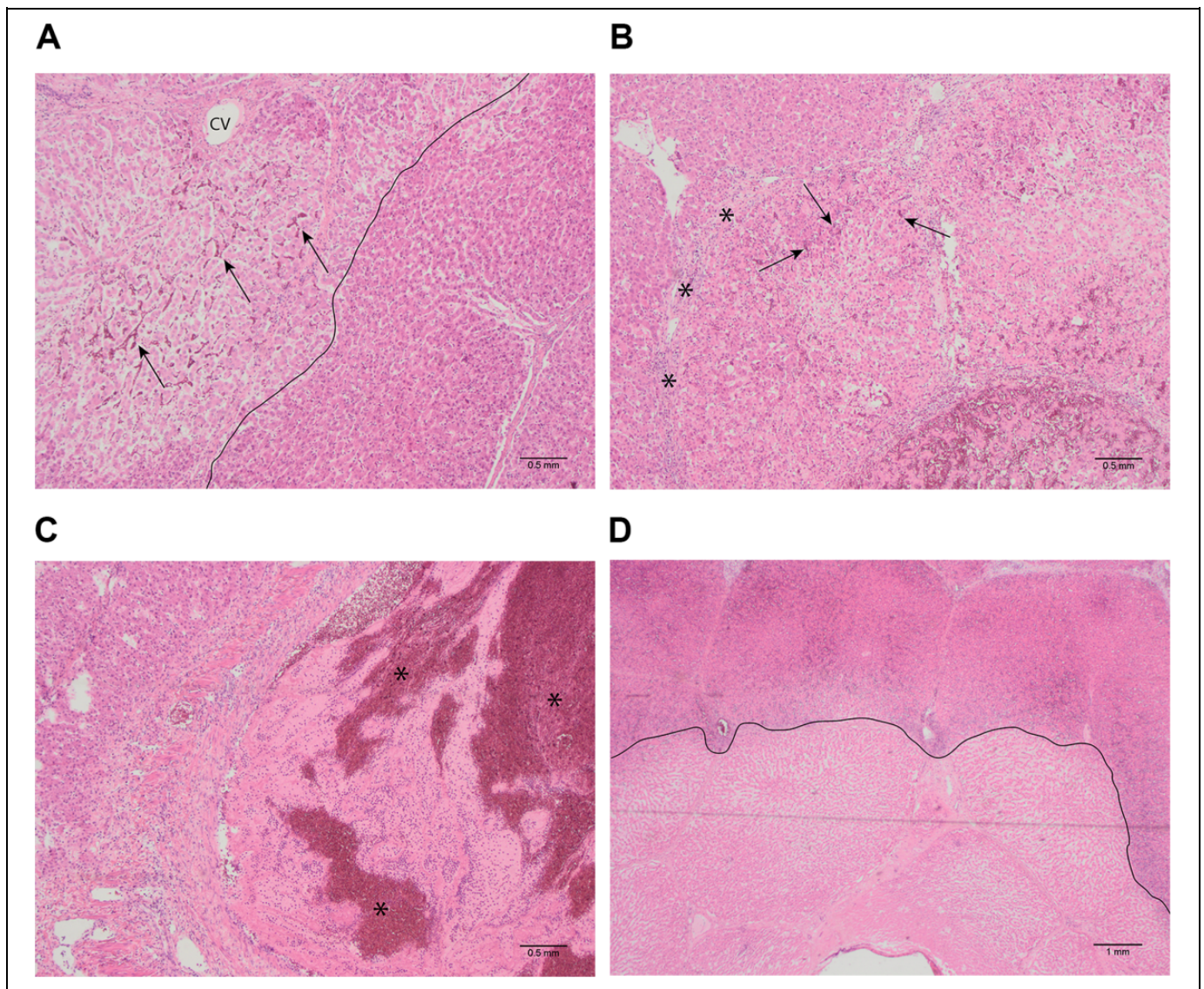


Figure 7. Hematoxylin-eosin stained liver sections at various time points post-IRE.

A, Liver section 1 hour after ablation, at 4× magnification shows a specific signs of cell death, such as eosinophilic cytoplasm and congestion of sinusoidal spaces. Arrows indicating congestion of sinusoidal spaces. CV: central vein. B, Liver section 4 hours after ablation, at 4× magnification shows moderate hemorrhagic infiltration and influx of neutrophils within the ablation zone. Arrows indicating hemorrhagic infiltration. Asterisks indicating neutrophilic infiltration. C, Liver section 8 hours after ablation, at 4× magnification shows a sharp demarcation of ablated and nonablated liver tissue and thrombosis of the liver microvasculature. Asterisks indicating thrombosis of microvasculature. D, Liver section 20 hours after ablation, at 2× magnification shows white coagulative necrosis of the tissue directly surrounding the electrodes. Delineated section indicating zone of white coagulative necrosis. IRE indicates irreversible electroporation.

a dynamic process with both gross pathologic and microscopic outcomes continuing for at least 24 hours. This has important implications for the design of future experimental and clinical studies assessing the impact of IRE.

In addition to previous (animal) experiments,¹⁴ our results show that IRE lesions (ie, ablation zones) significantly increase in size over 24 hours. As demonstrated in the present study, this impact may specifically account for the total ablation zone size but not the homogeneous zone with complete cell death. The increase in ablation zone volume could therefore mainly be attributed to an increase in size of the transition zone. This is

an important finding for future studies since histological assessment and/or imaging post-IRE may underestimate the total ablation zone size if performed within 24 hours after the ablation but can reliably determine whether the targeted area (ie, a tumor) is fully covered by the homogeneous ablation zone. We believe it is needed in clinical practice to cover an entire tumor within the homogeneous ablation zone, given the observed cell survival and thus chance of local recurrence within the transition zone.

The observed correlation between time and microscopic features of tissue damage, such as cell death and the initiation

of the inflammatory response, is grossly congruent with a recent systematic review.¹⁴ In short, only nonspecific histological changes are observed directly after ablation in previously performed studies reporting on IRE in liver in which yet after 1.5 to 2 hours, signs of cell death characteristic for both apoptosis as well as necrosis are seen.^{12,21,22} These pathological features of cell death are reported as pyknosis of nuclei, karyorrhexis, and condensation of hepatocyte cytoplasm.²³ This is followed by an inflammatory response, seen approximately 6 hours after ablation.^{21,22,24,25} These processes progress and stay present up to 72 hours following IRE, after which the damage is replaced by fibrosis.²⁶

The histological changes of the ablation zone following IRE treatment, as well as the contribution of time on the pathological response, show similarities with natural ischemic tissue damage (ie, brain/cardiac infarction).^{14,27} The ischemic tissue damage is initiated by nonspecific histological changes, such as dark basophilic nuclei or chromatin condensations (pyknosis), followed by advanced degeneration, cell death, and an inflammatory response.²⁷ In both cases, a waiting time is needed between tissue damage and histological evaluation, in order for the process of cell death to be completed. Although the time of onset of these features may vary between the causes of necrosis (IRE/ischemia) and tissue type, there are many similarities between IRE-induced tissue damage on one hand and ischemia leading to tissue infarction on the other hand. However, both characteristics of apoptosis and necrosis are seen while evaluating tissue effects of IRE,¹² leaving question marks regarding the true mechanism of cell death through IRE.

Moreover, in 2 cases, the distribution of the ablation zone showed heterogeneous results in relation to extent and shape of the IRE-induced lesions, even though the same settings (ie, voltage, pulse number, and duration) were used between the ablations. One of the contributing factors to shape and extent of the ablation zone may be the presence of large vascular structures and/or bile ducts within the ablated areas. As shown in Figure 5, gross pathological examination of the ablation zone shows an altered shape and size compared to the other lesions. This lesion is enclosed by 2 large vascular structures, which may have contributed to the redistribution of the electric field through electric field sink. It is demonstrated in an experiment by Goldberg *et al* that vessels within the ablation zone may contribute to an inhomogeneous distribution of the electric field, caused by electric field sink in the vessel wall.²⁸ However, multiple tissue samples show traversing blood vessels within or in close proximity of the ablation zone without signs of redistribution of the electric field; this was only the case for the lesion enclosed by 2 large (parallel) vascular structures. This may be of influence while performing IRE in unresectable tumors due to vascular involvement, where as a result of electricity sink an inhomogeneous distribution of the electric field could cause incomplete ablations or unintentionally ablate large areas of viable tissue.²⁸ Figure 8 shows one of the liver tissue samples with a large vascular structure within the ablated

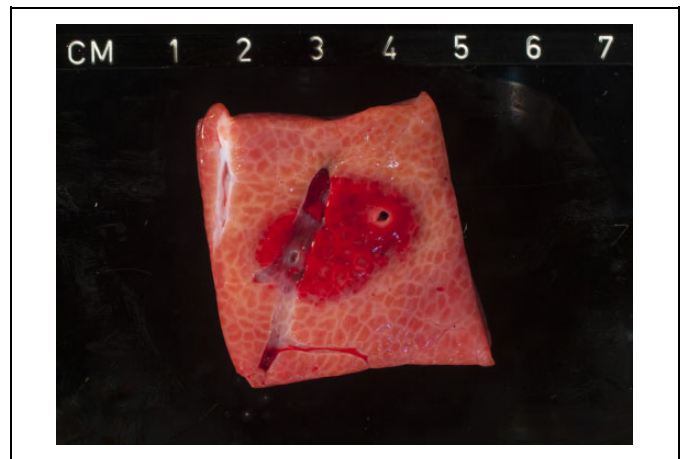


Figure 8. Gross-pathologic image 2 hours after IRE demonstrating large vascular structure traversing the ablation zone without signs of electric field sink or redistribution of the electric field.

region, without signs of redistribution of the electric field on gross pathological examination.

Furthermore, the areas of white coagulation surrounding the electrodes are presumably caused by thermal damage, whereas Van den Bos *et al* have demonstrated in an *in vitro* experiment that high temperatures can be reached surrounding the electrodes while using certain ablation parameters (ie, high electric field strength, pulse duration, and number of electrodes), sufficient to cause thermal damage.²⁹ Faroja *et al* correlated these observations with apoptotic activity, which is proven absent within these regions.¹² The presumed beneficial effect of IRE compared with contemporary focal ablation techniques, based on its nonthermal mechanism of work and cell death through apoptosis, may therefore be contentious. Careful treatment planning is warranted to avoid thermally vulnerable structures in the near presence of the electrode tips, where the largest increase in temperature is measured.²⁹

This study has some limitations. First, ablations were performed in healthy porcine liver. Pathologic tissue may therefore respond in a different way than is demonstrated in our results. Further research in pathologic tissue models is needed to optimize treatment with IRE and to demonstrate whether the progression of the ablation zone in pathologic tissue is comparable with the response in nonpathologic tissue. This may also account for varying tissue types, since the systematic review by Vogel *et al* demonstrated that histological response following IRE is also dependent on organ type.¹⁴ Second, this was a pilot study. Due to the relatively small number of ablations per time interval and multiple ablations per animal, the interindividual variation could have influenced the progression of the ablation zone and histological outcomes. Variation between animals may result in heterogeneity within the ablated tissue and thus cause a variety in electric field distribution. Moreover, it is unsure whether the multiple ablations in the same animal and long-term administration of anesthetics have influenced the outcomes. It can be hypothesized that the multiple ablations per animal could trigger a systemic response and hereby

influence the outcomes. This also accounts for the long-term administration of (inhalational) anesthetics since a previous study demonstrated that inhalational anesthetics may reduce the hepatic blood flow.³⁰ Tissue response may also vary between individuals, based on differences in inflammatory response and capability of tissue regeneration. A uniform model for standardization of the IRE ablation zones is needed, taking in consideration several factors such as the electrical tissue properties, IRE settings, and electrode configuration.

Conclusions

This is the first experimental study to assess the impact of time on tissue damage through IRE on the porcine liver during 24 consecutive hours. Both the pathological response (ie, cell death/inflammation) and ablation size are dynamic for at least 24 hours. Future studies should take this finding into account and may determine the impact of IRE after 24 hours, rather than the current 4 to 6 hours and should also determine the impact on pathological models.

Author Contribution

Jantien A. Vogel and Eran van Veldhuisen contributed equally to this work. Krijn P. van Lienden and Joanne Verheij share senior responsibility.

Ethical Statement

The study protocol was approved by the Animal Ethics Committee of the Academic Medical Center, Amsterdam (BEX 102047).

Declaration of Conflicting Interests

The author(s) declared the following potential conflicts of interest with respect to the research, authorship, and/or publication of this article: Krijn P. van Lienden and Thomas M. van Gulik are paid consultants for Angio-Dynamics.

Funding

The author(s) disclosed receipt of the following financial support for the research, authorship, and/or publication of this article: JA Vogel, E van Veldhuisen, OR Busch, TM van Gulik, MG Besselink and KP van Lienden received a grant (no. 2014-7244) from the Dutch Cancer Society (KWF) for studies on irreversible electroporation in pancreatic cancer.

ORCID iD

Eran van Veldhuisen  <https://orcid.org/0000-0002-5664-2286>

Supplemental Material

Supplemental material for this article is available online.

References

1. Neal RE, 2nd, Davalos RV. The feasibility of irreversible electroporation for the treatment of breast cancer and other heterogeneous systems. *Ann Biomed Eng.* 2009;37(12):2615-2625.
2. Martin RC, 2nd, Kwon D, Chalikhonda S, et al. Treatment of 200 locally advanced (stage III) pancreatic adenocarcinoma patients with irreversible electroporation: safety and efficacy. *Ann Surg.* 2015;262(3):486-494; discussion 492-484.
3. Narayanan G, Hosein PJ, Beulaygue IC, et al. Percutaneous image-guided irreversible electroporation for the treatment of unresectable, locally advanced pancreatic adenocarcinoma. *J Vasc Interv Radiol.* 2017;28(3):342-348.
4. Scheffer HJ, Vroomen LG, de Jong MC, et al. Ablation of locally advanced pancreatic cancer with percutaneous irreversible electroporation: results of the phase I/II PANFIRE study. *Radiology.* 2017;282(2):585-597.
5. Vogel JA, Rombouts SJ, de Rooij T, et al. Induction chemotherapy followed by resection or irreversible electroporation in locally advanced pancreatic cancer (IMPALA): a prospective cohort study. *Ann Surg Oncol.* 2017;24(9):2734-2743.
6. Scheffer HJ, Nielsen K, van Tilborg AA, et al. Ablation of colorectal liver metastases by irreversible electroporation: results of the COLDFIRE-I ablate-and-resect study. *Eur Radiol.* 2014;24(10):2467-2475.
7. Thomson KR, Cheung W, Ellis SJ, et al. Investigation of the safety of irreversible electroporation in humans. *J Vasc Interv Radiol.* 2011;22(5):611-621.
8. Coelen RJS, Vogel JA, Vroomen L, et al. Ablation with irreversible electroporation in patients with advanced perihilar cholangiocarcinoma (ALPACA): a multicentre phase I/II feasibility study protocol. *BMJ Open.* 2017;7(9):e015810.
9. Buijs M, van Lienden KP, Wagstaff PG, et al. Irreversible electroporation for the ablation of renal cell carcinoma: a prospective, human, in vivo study protocol (IDEAL phase 2b). *JMIR Res Protoc.* 2017;6(2):e21.
10. Scheltema MJ, van den Bos W, de Bruin DM, et al. Focal vs extended ablation in localized prostate cancer with irreversible electroporation; a multi-center randomized controlled trial. *BMC Cancer.* 2016;16:299.
11. Van den Bos W, Scheltema MJ, Siriwardana AR, et al. Focal irreversible electroporation as primary treatment for localized prostate cancer. *BJU Int.* 2017;121(5):716-724.
12. Faroja M, Ahmed M, Appelbaum L, et al. Irreversible electroporation ablation: is all the damage nonthermal? *Radiology.* 2013;266(2):462-470.
13. Golberg A, Yarmush ML. Nonthermal irreversible electroporation: fundamentals, applications, and challenges. *IEEE Trans Biomed Eng.* 2013;60(3):707-714.
14. Vogel JA, van Veldhuisen E, Agnass P, et al. Time-dependent impact of irreversible electroporation on pancreas, liver, blood vessels and nerves: a systematic review of experimental studies. *PLoS One.* 2016;11(11):e0166987.
15. Au JT, Mittra A, Song TJ, et al. Irreversible electroporation facilitates gene transfer of a GM-CSF plasmid with a local and systemic response. *Surgery.* 2013;154(3):496-503.
16. Au JT, Wong J, Mittra A, et al. Irreversible electroporation is a surgical ablation technique that enhances gene transfer. *Surgery.* 2011;150(3):474-479.
17. Charpentier KP, Wolf F, Noble L, Winn B, Resnick M, Dupuy DE. Irreversible electroporation of the liver and liver hilum in swine. *HPB (Oxford).* 2011;13(3):168-173.
18. Niessen C, Igl J, Pregler B, et al. Factors associated with short-term local recurrence of liver cancer after percutaneous ablation

- using irreversible electroporation: a prospective single-center study. *J Vasc Interv Radiol*. 2015;26(5):694-702.
19. Philips P, Hays D, Martin RC. Irreversible electroporation ablation (IRE) of unresectable soft tissue tumors: learning curve evaluation in the first 150 patients treated. *Plos One*. 2013;8(11): e76260.
 20. Martin RC, 2nd, Durham AN, Besselink MG, et al. Irreversible electroporation in locally advanced pancreatic cancer: a call for standardization of energy delivery. *J Surg Oncol*. 2016;114(7): 865-871.
 21. Ben-David E, Appelbaum L, Sosna J, Nissenbaum I, Goldberg SN. Characterization of irreversible electroporation ablation in in vivo porcine liver. *AJR Am J Roentgenol*. 2012;198(1): W62-68.
 22. Sugimoto K, Moriyasu F, Kobayashi Y, et al. Assessment of various types of US findings after irreversible electroporation in porcine liver: comparison with radiofrequency ablation. *J Vasc Interv Radiol*. 2015;26(2):279-287.e273.
 23. Elmore S. Apoptosis: a review of programmed cell death. *Toxicol Pathol*. 2007;35(4):495-516.
 24. Lee YJ, Lu DSK, Osuagwu F, Lassman C. Irreversible electroporation in porcine liver: short-and long-term effect on the hepatic veins and adjacent tissue by ct with pathological correlation. *Invest Radiol*. 2012;47(11):671-675.
 25. Liu Y, Xiong Z, Zhou W, Hua Y, Li C, Yao C. Percutaneous ultrasound-guided irreversible electroporation: a goat liver study. *Oncol Lett*. 2012;4(3):450-454.
 26. Lee EW, Chen C, Prieto VE, Dry SM, Loh CT, Kee ST. Advanced hepatic ablation technique for creating complete cell death: irreversible electroporation. *Radiology*. 2010;255(2):426-433.
 27. Margaritescu O, Mogoanta L, Pirici I, Pirici D, Cernea D, Margaritescu C. Histopathological changes in acute ischemic stroke. *Rom J Morphol Embryol*. 2009;50(3):327-339.
 28. Golberg A, Bruinsma BG, Uygun BE, Yarmush ML. Tissue heterogeneity in structure and conductivity contribute to cell survival during irreversible electroporation ablation by "electric field sinks". *Sci Rep*. 2015;5:8485.
 29. van den Bos W, Scheffer HJ, Vogel JA, et al. Thermal energy during irreversible electroporation and the influence of different ablation parameters. *J Vasc Interv Radiol*. 2016;27(3):433-443.
 30. Frink EJ, Jr., Morgan SE, Coetzee A, Conzen PF, Brown BR Jr. The effects of sevoflurane, halothane, enflurane, and isoflurane on hepatic blood flow and oxygenation in chronically instrumented greyhound dogs. *Anesthesiology*. 1992;76(1):85-90.